OPTICS

Scalable electrochromic nanopixels using plasmonics

Jialong Peng[1]*, Hyeon-Ho Jeong[1]*, Qianqi Lin[1], Sean Cormier[1], Hsin-Ling Liang[2], Michael F. L. De Volder[2], Silvia Vignolini[3], Jeremy J. Baumberg[1†]

Plasmonic metasurfaces are a promising route for flat panel display applications due to their full color gamut and high spatial resolution. However, this plasmonic coloration cannot be readily tuned and requires expensive lithographic techniques. Here, we present scalable electrically driven color-changing metasurfaces constructed using a bottom-up solution process that controls the crucial plasmonic gaps and fills them with an active medium. Electrochromic nanoparticles are coated onto a metallic mirror, providing the smallest-area active plasmonic pixels to date. These nanopixels show strong scattering colors and are electrically tunable across >100-nm wavelength ranges. Their bistable behavior (with persistence times exceeding hundreds of seconds) and ultralow energy consumption (9 fJ per pixel) offer vivid, uniform, nonfading color that can be tuned at high refresh rates (>50 Hz) and optical contrast (>50%). These dynamics scale from the single nanoparticle level to multicentimeter scale films in subwavelength thickness devices, which are a hundredfold thinner than current displays.

INTRODUCTION

Plasmonic resonances supported by noble metal nanostructures have emerged as an effective tool supporting a wide variety of enhanced optical phenomena (*1*), leading to applications such as sensing (*2*), imaging (*3*), actuation (*4*), and display (*5*–*8*). The latter is particularly interesting, as recent advances in nanolithography provide complex plasmonic building blocks that generate a rich set of colors while keeping their overall size smaller than pixels used in commercial displays. However, so far, their manufacture has been limited to the production of static colors obtained by complex arrangements of scattering elements to overcome the dependence on light polarization as well as illumination and viewing angles (*3*, *5*).

Active plasmonic colors can be obtained when the optical properties of the surrounding media are controlled by an applied stimulus (*5*). Plasmonic metasurfaces combined with electrochromic materials, including conductive polymers and phase-change materials, typically show on/off switching when the charge state of the electrochromic material changes (*9*–*11*). So far, these combinations enhance refresh rates and optical contrast by up to twofold compared to the electrochromic materials alone (*12*). Because the size of the plasmonic elements sets the RGB pixels for color generation (see table S1), (electro-)chemical means have been used to make plasmonic nanoparticles function as small optical switches/pixels. For instance, Au nanostructures coated with Ag shells show wide color dynamics through electrochemical control of the Ag shell thickness or redox state (*7*, *13*), but they suffer from very poor long-term reproducibility (<1 month) (*14*) and slow switching speeds (>0.5 s) (*13*). This is because when Ag is repeatedly stripped/redeposited (*7*) or oxidized/reduced (*13*), the ionic diffusion is slow and leads to rapid nanoscale morphological changes. Another approach is to combine plasmonic nanoparticles with conductive polymers (*15*–*17*). Although several such hybrid systems show faster reproducible dynamics, their resonant spectral features are shifted to the infrared, thus unsuited for display applications (see below for details).

A promising scheme to address these challenges is a multilayered plasmonic composite architecture filled with a dielectric spacer, known as the nanoparticle-on-mirror (NPoM). These can be constructed by "lithography-free" methods to subnanometer precision (*18*). The key feature is that the nanoparticles strongly confine light within their individual gaps to the underlying mirror and thus produce extremely localized cavity resonances (Fig. 1), making them independent and insensitive to the angle and polarization of the incident light. These features thus lend themselves to creating nanoscale pigments (*19*), but so far, no active color generation with NPoM geometries has fulfilled the requirements for display applications. The challenge lies in producing these NPoMs at large scale while ensuring that each individual NPoM acts as an independent active nanopixel.

Here, we report electrochromic nanoparticle-on-mirror constructs (*e*NPoMs) formed from gold nanoparticles (Au NPs) encapsulated in a conductive polymer shell [here polyaniline (PANI)]. Our scheme works by switching the charge state of the entire PANI shell, thus rapidly shifting the resonant scattering color of the *e*NPoM across >100-nm wavelength ranges. This active nanopixel only requires ~0.2 fJ of energy for each 1-nm shift in wavelength and can achieve commercial video rates (*20*). We show that centimeter-scale *e*NPoM metasurfaces assembled into disordered patterns by a scalable directed self-assembly scheme show vivid uniform color dynamics, not possible with any existing plasmonic color system.

RESULTS

Concept of *e*NPoM

Color dynamics based on a local surface plasmon resonance (LSPR) operates by changing the refractive index of the medium surrounding the plasmonic nanomaterial, shifting the LSPR peak position (*5*). The corresponding color tuning can be estimated from the LSPR sensitivity (*21*)

$$S_n = \frac{\Delta\lambda^*}{\Delta n} = \frac{-2\chi n}{(d\varepsilon_m/d\lambda)_{\lambda^*}} \quad (1)$$

where λ^* is the resonant wavelength, χ is a shape factor of the metal nanoparticle ($\chi = 2$ for spheres), ε_m is the dielectric permittivity of the metal nanoparticle, and n is the refractive index of the medium

[1]NanoPhotonics Centre, Cavendish Laboratory, University of Cambridge, Cambridge CB3 0HE, UK. [2]NanoManufacturing Group, Department of Engineering, University of Cambridge, Cambridge CB3 0FS, UK. [3]Bio-inspired Photonics Group, Department of Chemistry, University of Cambridge, Cambridge CB2 1EW, UK.
*These authors contributed equally to this work.
†Corresponding author. Email: jjb12@cam.ac.uk

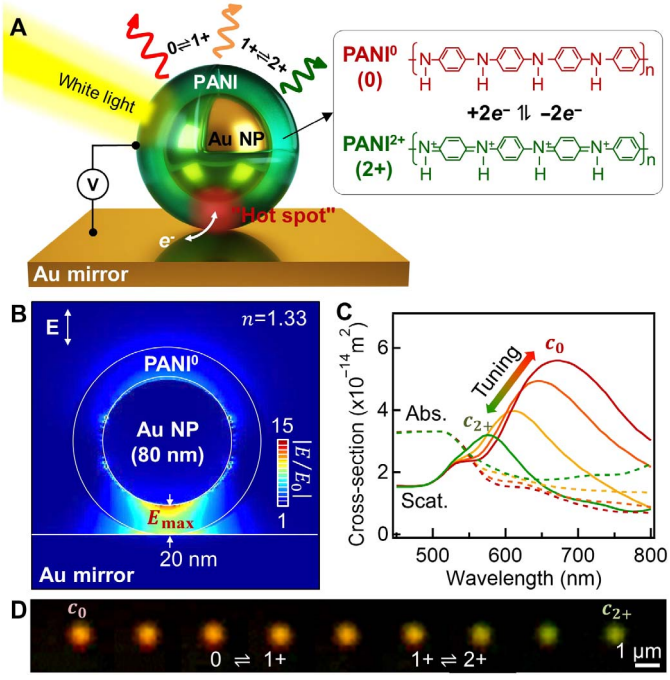

Fig. 1. *e*NPoM nanopixel. (**A**) Schematic of an *e*NPoM, which changes color as a function of redox state of the thin (0 to 20 nm) PANI shell surrounding each Au NP on Au mirror substrate. Right: Redox reaction of PANI in the gap ($PANI^0$, fully reduced; $PANI^{1+}$, half oxidized; $PANI^{2+}$, fully oxidized). (**B**) Optical near-field enhancement of the *e*NPoM for reduced state of PANI shell ($PANI^0$) showing hot spot in gap and (**C**) its corresponding optical scattering (solid lines) and absorption spectra (dashed lines) for different redox states of the PANI shell (red to green: $PANI^0$ to $PANI^{2+}$), from numerical simulations (see Materials and Methods). (**D**) Experimental dark-field (DF) scattering images of a single *e*NPoM nanopixel for different redox states of the PANI shell (left to right: $PANI^0$ to $PANI^{2+}$).

surrounding the nanoparticle. Ideally, Δn should be large while ensuring $n \sim 1$ to keep the LSPR resonance in the middle of the visible region and allowing $\Delta\lambda^*$ to tune over the whole visible spectrum.

A rational approach to address this is to incorporate plasmonic nanoparticles into active surroundings that change their optical properties (Δn) depending on external stimuli (*22*). Phase-change inorganic materials that have large Δn are one promising set of candidates (*23*), but because most have $n > 2$, their LSPR resonances are in the near infrared (NIR) and are thus inappropriate for plasmonic color applications. In contrast, responsive polymers offer LSPR modes in the visible as typically $n < 1.7$ (*24*) but show weak tuning ($\Delta n < 1$). Typical strategies used to achieve full color dynamics have thus combined responsive polymers with increased shape factors of the nanoparticles ($\chi > 2$) to increase S_n (Eq. 1). Elongated particles such as nanorods and bipyramids have higher χ, yielding higher $\Delta\lambda^*$ (*15*). However, these systems not only require large effective volumes (reducing the resolution) but also develop strong polarization-dependent resonances tuned beyond the visible regime into the NIR.

Here, we instead use *e*NPoMs composed of a Au NP encapsulated in a continuous PANI shell sitting just above a metallic mirror (Fig. 1A). This NPoM geometry behaves similarly to a dimer pair of near-touching plasmonic nanoparticles, giving rise to strong optical field coupling in the gap, known as a "hot spot" (Fig. 1B) (*1*). This hot spot leads to a strong additional coupled resonance (here mode *c*), together with a transverse mode around 550 nm supported by the Au NP alone (*2*). This coupled resonance tunes when the surrounding optical environment changes, while the transverse mode is only weakly affected. Furthermore, the coupled mode is insensitive to incident light polarization and angle, making this ideal for an extremely localized nanopixel (*18*). Here, this coupled resonance is tuned by changing the redox state of the ultrasmall volume of PANI shell surrounding each nanoparticle (~3×10^{-4} μm^3 per nanoparticle), altering the PANI molecular polarizability and thus its effective refractive index as much as $\Delta n = 0.6$ during redox (*25*).

Finite-difference time-domain (FDTD) numerical simulations (Fig. 1C) suggest that full redox of the PANI in the *e*NPoM can result in visible scattering wavelength shifts of >100 nm, 300% larger than those supported by nanoparticles alone (fig. S1, A to C) (*15*). In the reduced state of $PANI^0$, the *e*NPoM coupled resonance is at c_0 = 675 nm, which would blue-shift to c_{2+} = 575 nm when oxidized to $PANI^{2+}$. A helpful feature here is that *e*NPoMs with relatively large gaps (20-nm-thick PANI layer in Fig. 1C) still present useful color properties, compared to previous NPoMs with ultrathin dielectric spacers on a mirror (*2*, *18*, *19*). Contributions from the enhanced optical fields on top of each *e*NPoM double the $\Delta\lambda^*$ compared to NPoMs depending only on changes in their gap (see fig. S1, D to E, for details). Scattering supported by the optimal *e*NPoM predicts a 100-nm color range with 43% switching contrast at resonance (Fig. 1C), as well as >400% stronger scattering than absorption at resonance. This therefore promises a switchable color appearance with low optical loss as well as high spatial definition, confirmed in our experiments on single nanopixel devices (Fig. 1D).

Fabrication and optical switching of *e*NPoMs

Fabrication consists of two bottom-up steps: (i) PANI coating around colloidal Au NPs in solution and (ii) their casting onto a planar Au mirror (see Materials and Methods for details). In brief, the colloidal Au NPs are encapsulated by a continuous thin PANI shell using surfactant-assisted chemical oxidative polymerization (resulting particles shown in the inset of Fig. 2B) (*17*). These constructs constitute the key nanobuilding block controlling the optical resonance and its electron dynamics for redox chemistry. The shell thickness defines the critical gap spacing to the underlying mirror while also spacing between the neighboring Au NPs, reducing their optical coupling and inhibiting their aggregation. The electrochromic nanoparticles can be simply drop-cast onto planar Au substrates, resulting in randomly distributed *e*NPoMs but with extremely precise gap sizes (fig. S2). To scale this up in a controllable manner, meniscus-guided nanoparticle assembly is used here (*26*), which is robust and readily allows low-cost scalable fabrication of *e*NPoM metasurfaces with the desired surface coverage (see below).

These samples are integrated into custom-built electrochemical cells optimized to simultaneously track both optical and electrical dynamics via single-particle dark-field (DF) scattering spectroscopy combined with a potentiostat (fig. S2A). The Au mirror forms the working electrode (see Materials and Methods) (*27*), and the redox state of the PANI shells is controlled by sweeping the voltage from −0.2 to 0.6 V (versus Ag/AgCl) with a scan rate of 50 mV/s. Cyclic voltammetry (CV) curves averaged over 90 cycles (Fig. 2A) show two sets of oxidized (upper) and reduced peaks (lower) from the three different redox forms of PANI ($PANI^0$, fully reduced; $PANI^{1+}$, half oxidized; $PANI^{2+}$, fully oxidized). These *e*NPoMs are thus fully oxidized and reduced within only $\Delta V < 1$ V potential range. Simultaneously, DF scattering spectra of a single *e*NPoM are measured (Fig. 2B and Fig. 1D show corresponding DF images; see also movie S1 and fig. S2, C to E). Application of negative potential causes the reduction of the PANI shell

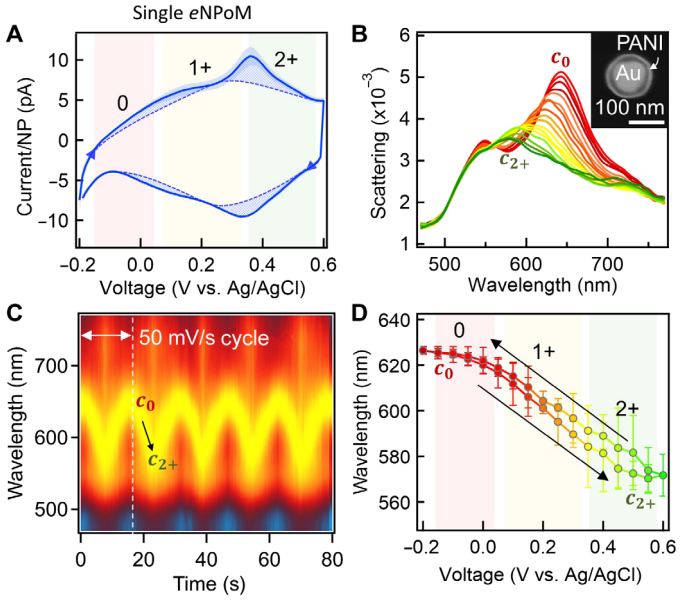

Fig. 2. Electrically driven optical switching of single *e*NPoMs. (**A**) Cyclic voltammetry (CV) of *e*NPoMs, with current calibrated per *e*NPoM (0, $PANI^0$; 1+, $PANI^{1+}$; 2+, $PANI^{2+}$; dashed background curve highlights redox peaks). (**B**) DF scattering spectra of single *e*NPoM versus voltage applied as in (A) (c_0, $PANI^0$; c_{2+}, $PANI^{2+}$). Inset shows SEM image of a representative *e*NPoM (80-nm Au NP coated with 20-nm PANI shell on Au substrate). (**C**) Time scan of normalized DF scattering spectra from a single *e*NPoM for five cycles of ramped voltage −0.2 ↔ 0.6 V with a scan rate of 50 mV/s. (**D**) Reversible switching of coupled plasmon mode versus applied voltage.

($PANI^0$), which gives rise to the scattering peak at c_0 = 642 nm. Reversing the potential reveals the resonance shift to c_{2+} = 578 nm, with $\Delta\lambda^*$ = 64 nm consistent with our numerical simulations (Fig. 1C). Further observations of the DF scattering spectra while undergoing CV cycling show highly stable and reversible optical switching (Fig. 2C) with dynamics that are fully reproducible (Fig. 2D). The optical dynamics of each *e*NPoM are found to be identical under the same conditions, a crucial basis for large-scale uniform color-switching metasurfaces based on this concept.

*e*NPoMs with varying gaps

To examine how *e*NPoM color switching is sensitive to structural parameters, we fabricate a series of *e*NPoMs with various gaps, set by the thicknesses of the PANI shell coated onto each Au NP. This is increased from 10- to 20-nm thickness with nanometer accuracy by controlling the monomer concentration used in the polymerization process (see Materials and Methods). The diameters are cross-checked (fig. S3) by scanning electron microscopy (SEM) and dynamic light scattering (DLS). We then fabricate *e*NPoM nanopixels from four different PANI thicknesses of 11, 13, 18, and 20 nm (Fig. 3A) and evaluate their electrical (Fig. 3B) and optical dynamics (Fig. 3, C to F, and movie S2 show real-time DF scattering images). Both simulated and experimental results for the spectral tuning as a function of the PANI shell thickness show characteristic reversible blue shifts (Fig. 3D) and ~50% intensity decrease (Fig. 3E) upon oxidation. In theory, the resonant wavelength and the range of its spectral tuning both increase for smaller gaps (shells). However, the experimental results show that thinner PANI shells result in a smaller color range upon redox cycling. This may be due to a number of additional geometrical factors not included in the simulations (which are extremely sensitive to the nanostructure) including (i) imperfect spherical shapes and sizes of the synthesized Au NPs (*28*), (ii) differences in optical properties of PANI of different thicknesses from additional effects of their ligands (*17*), (iii) nonuniform coatings of thinner PANI shells (<15 nm; Fig. 3A), (iv) the ~30% PANI thickness change during redox (*25*), and (v) possible nonuniform redox of PANI molecules within the gap, limiting the change of effective refractive index and thus the color dynamic range (fig. S4). This additional nanostructural control is of interest for electrical switching of extremely small gap plasmonic systems (*27*, *29*, *30*) but beyond the scope of this paper. In summary, the NPoMs made of thicker PANI shells (>15 nm) provide excellent color performance with high fidelity, in reasonable agreement with the optimal predictions of the numerical simulation.

Tracking reversible redox state from electronic and optical dynamics

The observed color change while switching the redox state of the conductive polymer opens up the ability to track the associated electron dynamics within the tiny channel underneath individual single nanoparticles in the NPoM geometry (Fig. 4A). This allows further insight into how many, and how fast, electrons can be transferred through the gap of an *e*NPoM. This is important for various applications, in particular fast and energy-efficient display devices (*12*), as well as for fundamental nano(electro-)chemistry (*31*, *32*).

With the *e*NPoM construct here, the redox species (PANI) is adsorbed onto the working electrode (the underlying Au mirror). The electron transfer between PANI and Au mirror is fast, as it occurs solely through the nanogap with negligible mass transport involved, ensuring the redox system is electrochemically reversible (*33*). The peak current i_P in the CV curve at the oxidized (or reduced) state of the *e*NPoMs is linearly proportional to the potential scan rate ν, with limited peak shift (fig. S5). In this case, $i_P = \nu F^2 fA/RT$, with two electrons involved, and where F is the Faraday constant (C/mol), R is the ideal gas constant (J/K·mol), T is the temperature of the system (K), A is the working electrode area (m^2), and f is the surface coverage of the species on the electrode (mol/m^2) (*33*). Because our experiments follow this linear dependence with ν, it shows that f is constant and gives the number of PANI molecules undergoing electron transfer (*34*), which is set by the number of *e*NPoMs on the electrode that we extract from the gradient fit (line). This then allows calibration of the number of electrons injected/collected from each NPoM (Fig. 4B), directly showing the electron dynamics in the gaps of single NPoMs associated with the three different redox states of the PANI. Roughly 30,000 e^- are transferred per nanoparticle, which is consistent with what is expected from the PANI shell volume (fig. S5E). The corresponding optical dynamics measured at the same time also show two clear transitions perfectly correlated to the electron dynamics (Fig. 4C, with fig. S5 showing detailed CV and DF spectra). These observations imply that the energies required for color changes from c_0 to c_{1+} and c_{1+} to c_{2+}, are ~80 and ~200 aJ per 1-nm shift in wavelength.

To understand the temporal response, we studied the optical switching of single *e*NPoMs under faster square-wave electrical modulation (Fig. 4D, top). An abrupt redox transition of the polymer is seen when a step in voltage from 0.6 ↔ −0.2 V is applied (versus Ag/AgCl), causing rapid shifts in the coupled mode from $c_0 \leftrightarrow c_{2+}$, and resulting in switching of the DF scattering measured at c_0 = 640 nm (Fig. 4D, bottom). The switching time is 32 ms (oxidation) and 143 ms (reduction) with intensity changes of 47%. This matches the intrinsic

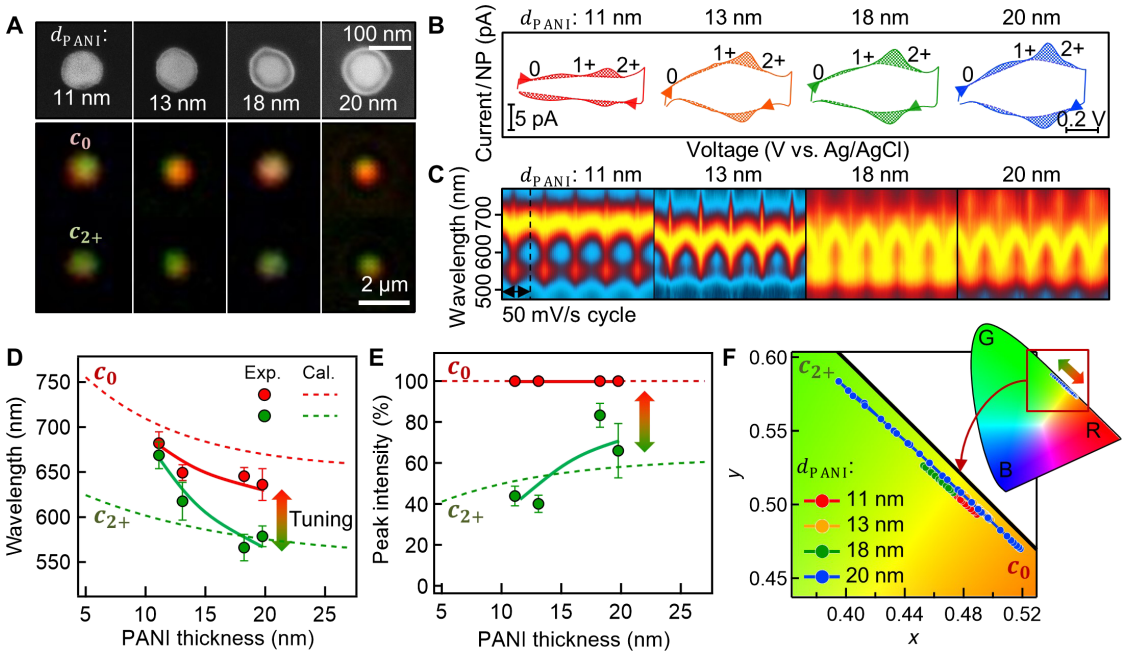

Fig. 3. *e*NPoMs with varying gaps. (**A**) Top: SEM images of Au NPs coated with different thicknesses of surrounding PANI shell layer (11, 13, 18, and 20 nm from left to right). Bottom: Corresponding DF images (top, $PANI^0$; bottom, $PANI^{2+}$). (**B**) CV curves of four different *e*NPoMs composed of 11-nm (red), 13-nm (orange), 18-nm (green), and 20-nm PANI shells (blue) versus applied voltage (from left to right). (**C**) Dynamic response in DF scattering of each NPoM nanopixel versus gap size. (**D**) Optical tuning (red, c_0; green, c_{2+}) and (**E**) corresponding intensity switching of *e*NPoMs as a function of PANI thickness (gap size) from theory (dashed lines) and experiment (circles and solid lines). (**F**) Associated color gamut plots (CIE 1931 chromaticity).

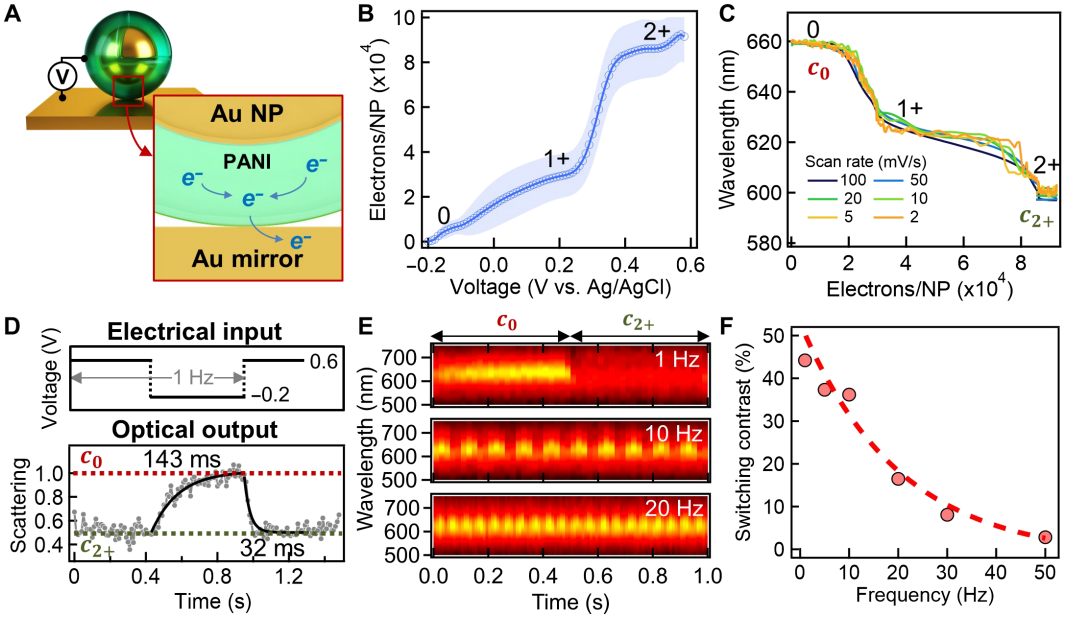

Fig. 4. Electrical and optical switching dynamics of *e*NPoM nanopixels. (**A**) Schematic of electron transfer from PANI to Au mirror through the gap. (**B**) Charge flow per nanoparticle in the gap of each *e*NPoM versus applied potential. (**C**) Optical dynamics of coupled plasmon mode versus number of electrons transferred at the gap. (**D**) Square-wave modulation of the applied potential at 1 Hz (top) and associated normalized scattering intensity (bottom) of single *e*NPoM at wavelength of c_0 peak, showing dynamics for reduction (143 ms) and oxidation (32 ms). (**E**) Reversible optical switching of an *e*NPoM under square-wave modulation at 1, 10, and 20 Hz. (**F**) Switching contrast of *e*NPoM versus applied modulation frequency.

dynamics of ultrathin planar PANI films on Au substrates (*12*), with >200% improved switching contrast in the enhanced scattering of the *e*NPoMs. Reversible color switching at the single nanoparticle level is seen in response to square-wave potentials of increasing frequency up to commercial video rates of 50 Hz (Fig. 4, E and F, with fig. S6 showing detailed performance) (*20*), providing switching performance that is already comparable to state of the art in plasmonics (*5*). The exponential decay in switching contrast for higher

frequencies currently comes from the RC time constant set by the resistance (R) and capacitance (C) of the cell geometry used.

Because PANI has stable charge states, we observe bistable characteristics for *e*NPoMs, with the resonant modes at c_{2+} and c_0 being retained for >10 min (decay time constant; fig. S6D). This therefore significantly reduces energy consumption for device applications. The retention time is currently limited by scavenger redox molecules and encapsulation that is not optimized in current devices but can be considerably extended. We emphasize that this is already 3×10^5 times extended compared to typical video rate refresh requirements.

Scalable *e*NPoM metasurfaces

In considering active plasmonics for industrial applications, one of the major challenges is scalable cost-effective fabrication of the functional metasurfaces, ideally based on lithography-free methods (*5*). We address this by developing a robust approach using meniscus-guided nanoparticle assembly to fabricate centimeter-scale *e*NPoM metasurfaces (Fig. 5; see Materials and Methods for details) (*26*). The volume fraction of the particles in solution used for the coating determines the particle density (fill fraction) on the mirror substrate. Surfaces composed of randomly distributed *e*NPoMs are achieved with fill fractions of 20% by using 0.3% volume fraction of the initial colloid (fig. S7). The corresponding ~100-nm spacing ensures minimal optical near-field coupling between the NPs (Fig. 5A), with colors controlled solely by the active gap under each *e*NPoM, and is essential for scalable fabrication. This scaled-up *e*NPoM metasurface also reveals vivid uniform color switching with $\Delta\lambda^* = 79$ nm and 57% switching contrast over the entire surface (Fig. 5, B to E). These observations are identical to the single *e*NPoM behavior, confirming the lack of any effects from the disordered configuration for fill fractions <20% (fig. S7) and giving metasurfaces fully insensitive to the light illumination and detection angles (fig. S8). The color ranges and dynamics supported by *e*NPoM metasurfaces can potentially be further extended by mixing different nanoparticles or using ultraviolet plasmonic nanoparticles (in progress).

The active plasmonic metasurface demonstrated here appears highly competitive with current and suggested technologies (Fig. 6) (*35*). In particular, it has visible wavelength tuning, ultrasmall pixel size, and near–video rate switching that has been hard to achieve before and matches requirements (green box). We emphasize that this metasurface already operates for over 3 months (Fig. 5F) at power densities below 300 μW/cm^2, which is 10 times lower than for commercial e-paper (fig. S9) while giving much higher pixel densities (>10^9 pixels per inch). This method is scalable and highly compatible with flexible systems and is therefore ideal for large-scale roll-to-roll manufacturing on deformable polymer substrates and suggests useful industrial applications for active plasmonic colors (*36*).

DISCUSSION

We demonstrate that combining conductive polymers into multilayered plasmonic architectures based on the NPoM architecture results in wide color switching in response to <1-V applied potentials. The tight confinement of light inside the well-defined and extremely small gap volumes allows independent tuning of the individual nanoparticles, which act as active nanopixels. Fast switching, high refresh rate, high optical contrast, low energy consumption, and the bistable characteristics of this hybrid nanoarchitecture are the key ingredients for creating scalable and flexible color-changing metasurfaces. Scattering-based color provided by single nanoparticles significantly increases the spatial resolution (<100 nm) while reducing the device thickness hundredfold compared to commercial high-definition displays (*12*) and simplifying the associated fabrication processes. These unique characteristics highlight its potential for active plasmonics in real-world applications including color-changing wallpapers, smart windows, traffic management systems, electrical signage, and many types of display panels.

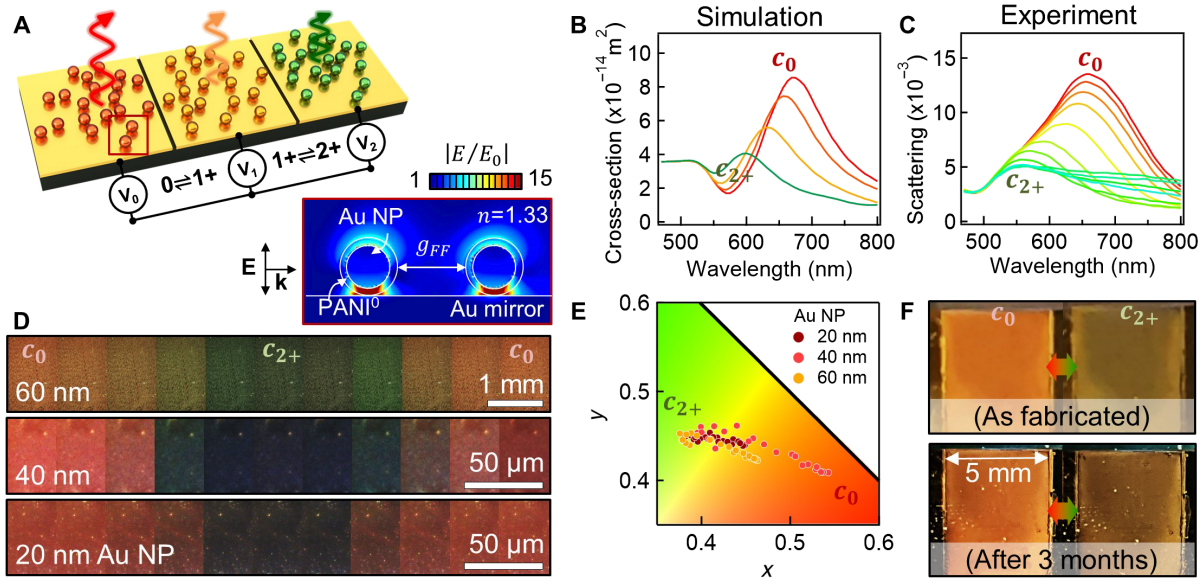

Fig. 5. Scalable color generation performance of *e*NPoM metasurfaces. (**A**) Schematic of *e*NPoM metasurface integrated into electrochemical cell. Right inset shows optical near-field enhancement of two *e*NPoMs built from 60-nm Au NPs, separated by mean distance g_{FF} = 90 nm (given 20% fill fraction), showing no optical near-field coupling between the *e*NPoMs. (**B**) Corresponding simulated spectra. (**C**) Experimental scattering spectra of the *e*NPoM metasurfaces versus voltage applied from −0.3 ↔ 0.8 V. (**D**) DF images and (**E**) color gamut (CIE 1931 chromaticity) of the *e*NPoM metasurfaces built from 20-, 40-, and 60-nm-diameter Au NPs during PANI redox. (**F**) Color dynamics of *e*NPoM metasurface from (C) under ambient light before and after 3 months. Photo credit: J. Peng and H.-H. Jeong, University of Cambridge.

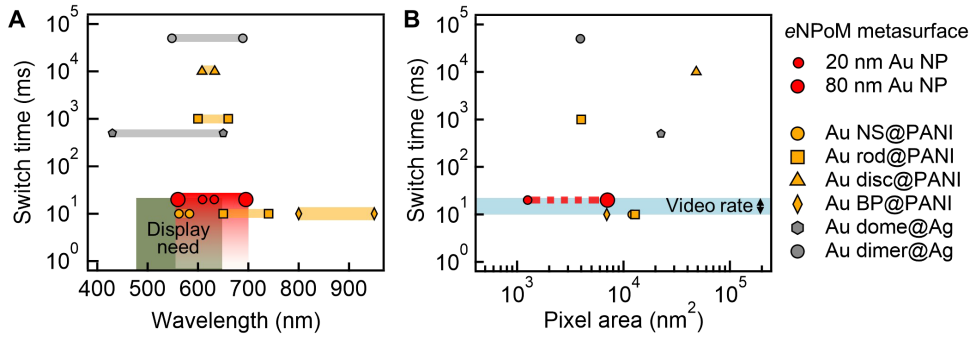

Fig. 6. Optical dynamics of electrochromic plasmonic nanoparticles. Switching times of various electrochromic plasmonic nanomaterials versus their associated (**A**) optical dynamic ranges and (**B**) pixel areas: *e*NPoMs (red circle), Au nanospheres (NS) coated with PANI (yellow circle), Au rods coated with PANI (yellow square), Au bipyramids (BP) coated with PANI (yellow bipyramid) (*15*), Au discs coated with PANI (yellow triangle) (*16*), Au domes coated with Ag (gray hexagon) (*7*), and Au dimers coated with Ag (gray circle) (*13*). Green box indicates needs for commercial displays, matching what can be achieved with *e*NPoMs (red).

Last, we note that besides these color display prospects, plasmonic color-changing metasurfaces offer diverse sensing functionalities. Because the optical properties of PANI are affected by changes in electronic charge as well as proton density (pH) (*37*), *e*NPoM metasurfaces can be used for flexible or wearable colorimetric sensors (*38*). Moreover, this scheme also has the potential for real-time measurements of hot-electron generation and photochemistry at extremely small length scales (*30*, *39*).

MATERIALS AND METHODS

PANI coating on Au NPs

PANI was coated on the surface of Au NPs by surfactant-assisted chemical oxidative polymerization, as previously reported (*15*, *17*). The citrate-stabilized colloidal solution (1.6 ml) of 80-nm Au NPs (BBI) was concentrated and mixed with a mixture of aniline (2 mM, 0.6 ml) and SDS (40 mM, 0.12 ml). Because of electrostatic forces, the aniline was coated onto the entire surface of the Au NPs, acting as a seed layer for further polymer growth. Then, 0.6 ml of 2 mM ammonium persulfate in 10 mM hydrochloric acid (HCl) was added into the solution. This led to polymerization of the monomers. For the complete polymerization, the solution was incubated at room temperature overnight and then washed and redispersed in 4 mM SDS solution afterward. The thickness of the PANI layer can be readily controlled by adjusting the amount of monomer in each coating procedure (fig. S3) or by repeating the whole process.

Preparation of *e*NPoM

Planar gold substrates were prepared by the template-stripping method reported in the literature, which provided atomically smooth gold layers (*28*). Briefly, 100-nm-thick Au was evaporated onto a silicon wafer at a growth rate of 0.1 nm/s using an e-beam evaporator. After this, small pieces (ca. 1 cm^2) of the bare Si wafer were glued on with epoxy and peeled off together with the Au film. Last, colloidal solutions of the PANI-coated Au NPs were drop-casted on the top of these Au substrates. Before use, this sample was immersed in deionized water overnight to eliminate excess surfactants, followed by treating with HCl (0.2 M) for 2 hours to protonate the PANI layer (*17*).

*e*NPoM metasurface coating

The coating of the *e*NPoM metasurface was carried out using a constructed convective coating setup (*26*). The evaporated Au substrate was cleaned with oxygen plasma and attached onto a motorized translation stage (ProScanII). A volume (ca. 40 μl) of the colloidal PANI-coated Au NPs was dropped onto the Au substrate. A fixed fluoro-silanized glass plate was positioned ~300 μm above the liquid to precisely confine the liquid during the coating. By moving the translation stage supporting the Au substrate at a constant speed of 1 μm/s, a liquid meniscus was formed on one edge and subsequently dragged across the substrate, accumulating and coating with nanoparticles. The fill fraction of the final metasurface was controlled by adjusting the volume fraction of the initial colloidal suspension.

DLS and SEM analysis

DLS spectra of the colloidal solutions (0.5 ml) of PANI-coated Au NPs were measured with a zeta potential analyzer (Zetasizer Nano ZS, Malvern), using the physical properties of Au and water. SEM images of the *e*NPoMs were obtained using a LEO 1530VP scanning electron microscope (Zeiss) at an accelerating voltage of 10 kV.

Single-particle optical DF imaging and spectroscopy

Optical DF images and spectra of single *e*NPoMs were obtained using a charge-coupled device camera (Infinity 2) and spectrometer (Ocean Optics QE65000) with 100× objectives [Olympus LMPLFLN; numerical aperture (NA), 0.8] in a customized microscope (Olympus BX51). The white light source is a halogen lamp.

Electrochemical cell

The Au mirror substrate of the *e*NPoM was used as a working electrode. A stack of square double-sided tape with the centers removed was adhered on a clean glass coverslip to create a fluid chamber. Half of the sample was sandwiched between two coverslips (see fig. S2), and the other half was electrically connected to a potentiostat (CompactStat, Ivium Technologies). A Ag/AgCl reference electrode (3M KCl, eDAQ ET072, Green Leaf Scientific) and a Pt counter electrode (Alfa Aesar) were inserted into the electrochemical cell, and the chamber was filled with the electrolyte solution [0.5 M sodium chloride (NaCl) in 10 mM HCl].

Numerical simulation

The electromagnetic response of the *e*NPoM was simulated by FDTD calculation software (Lumerical Solutions). The Au nanosphere surrounded with the spherical PANI shell was placed on top of a gold rectangular mirror. The light was illuminated as a plane wave polarized perpendicular to and propagating towards the mirror

(fig. S1). The optical properties of Au and PANI were taken from the literature (*25*, *40*). To simplify the computation, the refractive index of the whole surrounding environment was set to $n = 1.33$ assuming water.

SUPPLEMENTARY MATERIALS

Supplementary material for this article is available at http://advances.sciencemag.org/cgi/content/full/5/5/eaaw2205/DC1

Fig. S1. FDTD simulations of Au NPs and *e*NPoMs.
Fig. S2. Electrochemical cell.
Fig. S3. PANI coating on Au NPs with thickness control.
Fig. S4. FDTD numerical simulation of *e*NPoM for different redox states in the gap.
Fig. S5. Electrochemical analysis of *e*NPoMs.
Fig. S6. Reversible optical switching of *e*NPoMs.
Fig. S7. *e*NPoM metasurfaces.
Fig. S8. Angular dependence of *e*NPoM metasurfaces.
Fig. S9. Power density of various displays.
Table S1. Comparison of electrochromic plasmonic reflective devices.
Movie S1. Matrix (6 × 6) of the DF scattering images of the *e*NPoMs as a function of time during CV cycle in the range of −0.2 to 0.6 V (versus Ag/AgCl) with a scan rate of 50 mV/s.
Movie S2. DF scattering images of four different particles (in row) of four different *e*NPoMs composed of 11-, 13-, 18-, and 20-nm PANI thicknesses as a function of time during CV cycle in the range of −0.2 to 0.6 V (versus Ag/AgCl) with a scan rate of 50 mV/s.
Movie S3. DF scattering images of the *e*NPoM metasurfaces as a function of time during CV cycle in the range of −0.2 to 0.6 V (versus Ag/AgCl) with a scan rate of 50 mV/s.

REFERENCES AND NOTES

1. W. Zhu, R. Esteban, A. G. Borisov, J. J. Baumberg, P. Nordlander, H. J. Lezec, J. Aizpurua, K. B. Crozier, Quantum mechanical effects in plasmonic structures with subnanometre gaps. *Nat. Commun.* **7**, 11495 (2016).
2. R. Chikkaraddy, B. de Nijs, F. Benz, S. J. Barrow, O. A. Scherman, E. Rosta, A. Demetriadou, P. Fox, O. Hess, J. J. Baumberg, Single-molecule strong coupling at room temperature in plasmonic nanocavities. *Nature* **535**, 127–130 (2016).
3. A. Kristensen, J. K. W. Yang, S. I. Bozhevolnyi, S. Link, P. Nordlander, N. J. Halas, N. A. Mortensen, Plasmonic colour generation. *Nat. Rev. Mater.* **2**, 16088 (2016).
4. M. Liu, T. Zentgraf, Y. Liu, G. Bartal, X. Zhang, Light-driven nanoscale plasmonic motors. *Nat. Nanotechnol.* **5**, 570–573 (2010).
5. L. Shao, X. Zhuo, J. Wang, Advanced plasmonic materials for dynamic color display. *Adv. Mater.* **30**, 1704338 (2018).
6. J. Olson, A. Manjavacas, L. Liu, W.-S. Chang, B. Foerster, N. S. King, M. W. Knight, P. Nordlander, N. J. Halas, S. Link, Vivid, full-color aluminum plasmonic pixels. *Proc. Natl. Acad. Sci. U.S.A.* **111**, 14348–14353 (2014).
7. G. Wang, X. Chen, S. Liu, C. Wong, S. Chu, Mechanical chameleon through dynamic real-time plasmonic tuning. *ACS Nano* **10**, 1788–1794 (2016).
8. J. Li, S. Kamin, G. Zheng, F. Neubrech, S. Zhang, N. Liu, Addressable metasurfaces for dynamic holography and optical information encryption. *Sci. Adv.* **4**, eaar6768 (2018).
9. D. Franklin, R. Frank, S.-T. Wu, D. Chanda, Actively addressed single pixel full-colour plasmonic display. *Nat. Commun.* **8**, 15209 (2017).
10. K. Xiong, G. Emilsson, A. Maziz, X. Yang, L. Shao, E. W. H. Jager, A. B. Dahlin, Plasmonic metasurfaces with conjugated polymers for flexible electronic paper in color. *Adv. Mater.* **28**, 9956–9960 (2016).
11. K. Xiong, D. Tordera, G. Emilsson, O. Olsson, U. Linderhed, M. P. Jonsson, A. B. Dahlin, Switchable plasmonic metasurfaces with high chromaticity containing only abundant metals. *Nano Lett.* **17**, 7033–7039 (2017).
12. T. Xu, E. C. Walter, A. Agrawal, C. Bohn, J. Velmurugan, W. Zhu, H. J. Lezec, A. A. Talin, High-contrast and fast electrochromic switching enabled by plasmonics. *Nat. Commun.* **7**, 10479 (2016).
13. C. P. Byers, H. Zhang, D. F. Swearer, M. Yorulmaz, B. S. Hoener, D. Huang, A. Hoggard, W.-S. Chang, P. Mulvaney, E. Ringe, N. J. Halas, P. Nordlander, S. Link, C. F. Landes, From tunable core-shell nanoparticles to plasmonic drawbridges: Active control of nanoparticle optical properties. *Sci. Adv.* **1**, e1500988 (2015).
14. B. Molleman, T. Hiemstra, Time, pH, and size dependency of silver nanoparticle dissolution: The road to equilibrium. *Environ. Sci. Nano* **4**, 1314–1327 (2017).
15. W. Lu, N. Jiang, J. Wang, Active electrochemical plasmonic switching on polyaniline-coated gold nanocrystals. *Adv. Mater.* **29**, 1604862 (2017).
16. Y. Leroux, J. C. Lacroix, C. Fave, G. Trippe, N. Félidj, J. Aubard, A. Hohenau, J. R. Krenn, Tunable electrochemical switch of the optical properties of metallic nanoparticles. *ACS Nano* **2**, 728–732 (2008).
17. J.-W. Jeon, P. A. Ledin, J. A. Geldmeier, J. F. Ponder Jr., M. A. Mahmoud, M. el-Sayed, J. R. Reynolds, V. V. Tsukruk, Electrically controlled plasmonic behavior of gold Nanocube@Polyaniline nanostructures: Transparent plasmonic aggregates. *Chem. Mater.* **28**, 2868–2881 (2016).
18. A. Moreau, C. Ciracì, J. J. Mock, R. T. Hill, Q. Wang, B. J. Wiley, A. Chilkoti, D. R. Smith, Controlled-reflectance surfaces with film-coupled colloidal nanoantennas. *Nature* **492**, 86–89 (2012).
19. J. W. Stewart, G. M. Akselrod, D. R. Smith, M. H. Mikkelsen, Toward multispectral imaging with colloidal metasurface pixels. *Adv. Mater.* **29**, 1602971 (2017).
20. J. Davis, Y.-H. Hsieh, H.-C. Lee, Humans perceive flicker artifacts at 500 Hz. *Sci. Rep.* **5**, 7861 (2015).
21. M. M. Miller, A. A. Lazarides, Sensitivity of metal nanoparticle surface plasmon resonance to the dielectric environment. *J. Phys. Chem. B* **109**, 21556–21565 (2005).
22. I. Tokarev, S. Minko, Tunable plasmonic nanostructures from noble metal nanoparticles and stimuli-responsive polymers. *Soft Matter* **8**, 5980–5987 (2012).
23. M. Wuttig, H. Bhaskaran, T. Taubner, Phase-change materials for non-volatile photonic applications. *Nat. Photonics* **11**, 465–476 (2017).
24. W. Knoll, *Materials Science and Technology* (Wiley-VCH Verlag GmbH & Co. KGaA, 2006).
25. C. Barbero, R. Kotz, Nanoscale dimensional changes and optical properties of polyaniline measured by in situ spectroscopic ellipsometry. *J. Electrochem. Soc.* **141**, 859–865 (1994).
26. L. Malaquin, T. Kraus, H. Schmid, E. Delamarche, H. Wolf, Controlled particle placement through convective and capillary assembly. *Langmuir* **23**, 11513–11521 (2007).
27. G. Di Martino, V. A. Turek, A. Lombardi, I. Szabó, B. de Nijs, A. Kuhn, E. Rosta, J. J. Baumberg, Tracking nanoelectrochemistry using individual plasmonic nanocavities. *Nano Lett.* **17**, 4840–4845 (2017).
28. F. Benz, R. Chikkaraddy, A. Salmon, H. Ohadi, B. de Nijs, J. Mertens, C. Carnegie, R. W. Bowman, J. J. Baumberg, SERS of individual nanoparticles on a mirror: Size does matter, but so does shape. *J. Phys. Chem. Lett.* **7**, 2264–2269 (2016).
29. L. Cui, B. Liu, D. Vonlanthen, M. Mayor, Y. Fu, J.-F. Li, T. Wandlowski, In situ gap-mode raman spectroscopy on single-crystal Au(100) electrodes: Tuning the torsion angle of 4,4′-biphenyldithiols by an electrochemical gate field. *J. Am. Chem. Soc.* **133**, 7332–7335 (2011).
30. B. de Nijs, F. Benz, S. J. Barrow, D. O. Sigle, R. Chikkaraddy, A. Palma, C. Carnegie, M. Kamp, R. Sundararaman, P. Narang, O. A. Scherman, J. J. Baumberg, Plasmonic tunnel junctions for single-molecule redox chemistry. *Nat. Commun.* **8**, 994 (2017).
31. L. Zhou, D. F. Swearer, C. Zhang, H. Robatjazi, H. Zhao, L. Henderson, L. Dong, P. Christopher, E. A. Carter, P. Nordlander, N. J. Halas, Quantifying hot carrier and thermal contributions in plasmonic photocatalysis. *Science* **362**, 69–72 (2018).
32. E. Cortés, W. Xie, J. Cambiasso, A. S. Jermyn, R. Sundararaman, P. Narang, S. Schlücker, S. A. Maier, Plasmonic hot electron transport drives nano-localized chemistry. *Nat. Commun.* **8**, 14880 (2017).
33. N. Elgrishi, K. J. Rountree, B. D. McCarthy, E. S. Rountree, T. T. Eisenhart, J. L. Dempsey, A practical beginner's guide to cyclic voltammetry. *J. Chem. Educ.* **95**, 197–206 (2018).
34. H. S. Kolla, S. P. Surwade, X. Zhang, A. G. MacDiarmid, S. K. Manohar, Absolute molecular weight of polyaniline. *J. Am. Chem. Soc.* **127**, 16770–16771 (2005).
35. M. R. Fernández, E. Z. Casanova, I. G. Alonso, Review of display technologies focusing on power consumption. *Sustainability* **7**, 10854–10875 (2015).
36. S. Murthy, H. Pranov, N. A. Feidenhans'l, J. S. Madsen, P. E. Hansen, H. C. Pedersen, R. Taboryski, Plasmonic color metasurfaces fabricated by a high speed roll-to-roll method. *Nanoscale* **9**, 14280–14287 (2017).
37. E. Pringsheim, D. Zimin, O. S. Wolfbeis, Fluorescent beads coated with polyaniline: A novel nanomaterial for optical sensing of pH. *Adv. Mater.* **13**, 819–822 (2001).
38. T. Yokota, P. Zalar, M. Kaltenbrunner, H. Jinno, N. Matsuhisa, H. Kitanosako, Y. Tachibana, W. Yukita, M. Koizumi, T. Someya, Ultraflexible organic photonic skin. *Sci. Adv.* **2**, e1501856 (2016).
39. Y. Kim, J. G. Smith, P. K. Jain, Harvesting multiple electron-hole pairs generated through plasmonic excitation of Au nanoparticles. *Nat. Chem.* **10**, 763–769 (2018).
40. P. B. Johnson, R. W. Christy, Optical constants of the noble metals. *Phys. Rev. B* **6**, 4370–4379 (1972).

Acknowledgments: We are grateful to B. Nijs and R. Chikkaraddy for support with fabrication and simulations, as well as the NanoPhotonics Centre and the Nanoscience Centre at the University of Cambridge for technical support. **Funding:** We acknowledge EPSRC grants EP/N016920/1, EP/L027151/1, EP/P029426/1, and NanoDTC EP/L015978/1. H.-L.L. and S.V. acknowledge ERC grants ERC-PoC-2017_790518 PixCell and SeSaMe -ERC-2014-STG-639088. J.P. thanks the China Scholarship Council for Ph.D. funding. **Author contributions:** J.P., H.-H.J., and J.J.B. conceived and developed the experiments and developed electrochemistry (together with Q.L.) and growth and modeling (together with

S.C.). H.-L.L., M.F.L.D.V., and S.V. helped to develop scaled-up systems. **Competing interests:** J.J.B., H.-H.J., and J.P. are inventors on a UK patent application related to this work filed by the UK Patent Office (no. GB1903650.8; filed on 18 March 2019). The authors declare no other competing interests. **Data and materials availability:** All data needed to evaluate the conclusions in the paper are present in the paper and/or the Supplementary Materials. All source data related to this paper can be accessed at https://doi.org/10.17863/CAM.37021. Additional data related to this paper may be requested from the authors.

Submitted 30 November 2018
Accepted 27 March 2019
Published 10 May 2019
10.1126/sciadv.aaw2205

Citation: J. Peng, H.-H. Jeong, Q. Lin, S. Cormier, H.-L. Liang, M. F. L. De Volder, S. Vignolini, J. J. Baumberg, Scalable electrochromic nanopixels using plasmonics. *Sci. Adv.* **5**, eaaw2205 (2019).

Science Advances

Scalable electrochromic nanopixels using plasmonics

Jialong Peng, Hyeon-Ho Jeong, Qianqi Lin, Sean Cormier, Hsin-Ling Liang, Michael F. L. De Volder, Silvia Vignolini and Jeremy J. Baumberg

Sci Adv **5** (5), eaaw2205.
DOI: 10.1126/sciadv.aaw2205